The Influence of X-Rays on the Structural Studies of Peroxide-Derived Myoglobin Intermediates

Hersleth, Hans-Petter; Hsiao, Ya-Wen; Ryde, Ulf; Gorbitz, Carl Henrik; Andersson, K. Kristoffer

Published in:
Chemistry and Biodiversity

2008

Document Version:
Peer reviewed version (aka post-print)

The Influence of X-Rays on the Structural Studies of Peroxide-Derived Myoglobin Intermediates.

by **Hans-Petter Hersleth**[a][b], **Ya-Wen Hsiao**[c], **Ulf Ryde**[c], **Carl Henrik Görbitz**[b] and **K. Kristoffer Andersson***[a]

[a] University of Oslo, Department of Molecular Biosciences, P.O. Box 1041 Blindern, N-0316 Oslo, Norway

[b] University of Oslo, Department of Chemistry, P.O. Box 1033 Blindern, N-0315 Oslo, Norway

[c] Lund University, Department of Theoretical Chemistry, P.O. Box 124, S-221 00, Sweden.

*To whom correspondence should be addressed: K. Kristoffer Andersson, E-Mail: k.k.andersson@imbv.uio.no

ABSTRACT

In recent years the awareness of potential radiation damage of metal centres in protein crystals during crystallographic data collection has received increasing attention. The radiation damage can lead to radiation-induced changes and reduction of the metal sites. One of the research fields where these concerns have been comprehensively addressed is in the study of the reaction intermediates of the haem peroxidase and oxygenase reaction cycles. For both the resting states and the high-valent intermediates the X-rays used in the structural determination have given undesired side effects through radiation-induced changes to the trapped intermediates. However, X-rays have been used to generate and trap the peroxy/hydroperoxy state in crystals. In this review the structural work and the influence of X-rays on these intermediates in myoglobin are summarised and viewed in light of analogous studies on similar intermediates in peroxidases and oxygenases.

CONTENTS

1. Introduction.

Haem proteins are involved in several different process: catalysis, electron transfer, oxygen transport / storage and sensoring of the small inorganic molecules O_2, NO and CO [1-3]. The haem peroxidases, oxygenases and catalases catalyse different reactions (e.g. the one- or two-electron oxidation of substrates, hydroxylation and epoxidation of organic molecules, or conversion of hydrogen peroxide to molecular oxygen and water) [4-6]. Their reaction cycles are different, but several of the reaction intermediates are similar, and they have been extensively studied during the last 100 years. Several of these reaction intermediates have been determined with X-ray diffraction [7]. The increased awareness of potential radiation damage of the metal centre in haem proteins during crystallographic data collection has lead to several recent surveys combining the study of haem peroxidase and oxygenase intermediates and radiation damage studies [8-14]. The haem proteins are good candidates for such studies because of their characteristic absorption in the 350 to 700 nm wavelength range. Myoglobin (Mb) can (as will be described below) propagate through several of the similar intermediates as the peroxidases and oxygenases, and has been used as a model system for such intermediates. In this review the structural work and the influence of X-rays on these intermediates in Mb are summarised, and viewed in light of analogous studies on similar intermediates in peroxidases and oxygenases.

2. Myoglobin and the reaction with peroxide

The history of Mb dates back to 1775 with the first observation of the red pigment of muscle by Boerhaave, and the name myoglobin was first used by Günther in 1921 [15]. Mb is a haem protein found mainly in heart and skeletal muscle, and its main biological function is to buffer the oxygen concentration in respiring tissues by oxygen storage [16-18]. Mb has an affinity for oxygen that falls between that for haemoglobin (Hb) (which should release oxygen in respiring tissues) and cytochrome *c* oxidase (which use oxygen in oxidative respiration) [18]. More recently an understanding has evolved of Mb also as a protein with multiple functions such as protection against oxidative damage and NO scavenging as well as involvement in oxidative tissue damage [19-24].

It has been known from the 1950s that Mb can react with hydrogen peroxide and give a ferryl species in a peroxidase-style manner (but with important differences, as will be detailed below) [25-27]. For a classical peroxidase (like horseradish peroxidase, HRP), the reaction cycle

involves a two-electron oxidation-reduction (Peroxidase catalytic cycle in Scheme 1) with oxidation of organic molecules.

In the first HRP step the resting ferric (Fe^{III}) high-spin (S=5/2) form is oxidised by hydrogen peroxide to a water molecule and a haem state called compound I that is two oxidation equivalents higher than the resting ferric form. This first step propagates through an unstable hydroperoxy-intermediate (compound 0) where the compound I is generated through a heterolytic cleavage of the O-O bond [28-30]. In Mb both the hydroperoxy state and compound I are quite unstable, but have been observed under certain conditions [31-34]. The distal His is assumed to function as an acid/base catalyst to facilitate the heterolytic cleavage by accepting a proton from the inner oxygen (oxygen ligated to the iron) and then donating it to the outer (leaving) oxygen. The negative charge on the leaving hydroxide during bond cleavage is then stabilised by the distal Arg in HRP (not found in Mb) [35, 36]. Additionally, the proximal His can stabilise higher oxidation states on the haem iron by hydrogen bonding to a neighbouring carboxylate group, thus making the Fe-bound N more negative [35, 36]. The compound I intermediate formed is two oxidation equivalents higher than the resting form (Fe^{III}). One electron is withdrawn from the iron, resulting in a ferryl ($Fe^{IV}O$) state with a double-bonded oxygen atom and intermediate spin state (S=1), which could interact magnetically with radicals. Depending on the peroxidase, the second oxidising electron comes from either the porphyrin ring, giving a π-cation radical, or from an amino acid residue (Trp or Tyr) near the haem ring [6, 37]. In the second step of the peroxidase reaction cycle, compound I carries out a substrate (e.g. organic molecule A) oxidation ($A \rightarrow A^{+\bullet}$), which for the haem results in a one-electron reduction to compound II (S=1) by the loss of the haem/protein-radical. The last step of the cycle is a further one-electron reduction of the compound II to the resting ferric form, accompanied again by a second substrate oxidation ($A \rightarrow A^{+\bullet}$).

Mb can react with hydrogen peroxide in a manner similar to peroxidases, including oxidising several classes of small organic molecules, but at a much lower rate [38, 39]. The reduced efficiency can be explained by the lack of three essential residues; the Asp that forms the hydrogen bond to the proximal His, the distal Arg that stabilises the negative charge on the leaving group, and the distal His that is suggested to be too close to the haem to fully function as an acid-base catalyst during the heterolytic cleavage of the peroxide bond [33, 35, 36, 40]. Through mutation studies, Watanabe and co-workers showed that mimicking the His distance in

peroxidases increased the peroxidase activity of Mb and also led to the observation of compound I [33, 41, 42]. The peroxidase intermediates described above are also found in haem-based oxygenases and catalases even though their reaction cycles are different. Several crystal structures of these intermediates have been solved [7]. As mentioned above, active-site amino acids of peroxidases are involved in deprotonation/protonation of the iron-linked peroxide in the first step of the reaction cycle. In contrast, it appears that for the monooxygenases cytochrome P450 (P450), nitric oxide synthase (NOS) and haem oxygenase (HO), solvent molecules are responsible for the protonation of the dioxygen, leading to the cleavage of the O-O bond [43]. For P450 and NOS as well as for bromo- and chloroperoxidase (CPO) the proximal ligand is a Cys and for most catalases it is a Tyr. These three residues differ in their electron donating capability to the iron, which can lead to some differences between these enzymes [44].

In the presence of excess hydrogen peroxide an additional intermediate, compound III, is generated from compound II through reaction with another hydrogen peroxide molecule (Scheme 1) [26, 45-47]. Several of the states described above are quite labile for X-ray induced radiation damage during crystallographic data collection. In Scheme 1, the X-ray induced changes that have been observed for the different Mb states are shown: compound II changes to intermediate H (radiation-induced compound II), compound III to peroxyMb, and ferric metMb to aqua ferrous Mb.

3. Radiation damage to metalloproteins during crystallographic data collection.

In protein crystallography the diffraction data are regularly collected at cryogenic temperatures. However, radiation damage still occurs at 100 K [48, 49]. During the crystallographic data collection, only about 10% of the interacting X-ray photons at a wavelength of 1 Å are elastically scattered and give diffraction, while the rest of the interacting X-ray photons deposit their energy into the crystal lattice, where damage is induced, mostly through the photoelectric effect with generation of photoelectrons [50]. This can further lead to secondary electron emission, estimated to 10 000 electrons for each elastically scattered photon [50]. The general radiation damage is characterised by loss of resolution, increased B-factors, R_{sym}, mosacity, as well as disulfide-bond breakage and decarboxylation. Radiation damage leading to loss of useable data from crystallography was early recognised [51], and Henderson proposed a dose limits of 20 MGy for cryo-cooled protein crystals at which the diffracted intensity would be halved [52]. The

recommended dose limit for typical macromolecular crystallography experiments have recently been re-estimated to 30 MGy [53].

Active sites seem to be particularly vulnerable to radiation damage [54]. The generated reducing equivalents during the X-ray diffraction experiments can particularly reduce redox-active states in metalloproteins [9, 55, 56], and Beitlich *et al*. compare haem irons to "vacuum cleaners" sucking in electrons [8]. A technique is needed to monitor such potential radiation damage to the metal sites. For metalloproteins that absorb light in the UV-Vis region, the changes can be monitored by single-crystal light absorption spectroscopy (microspectrophotometry) [9, 50, 57, 58]. The different redox-states in haem proteins have characteristic light absorption in the 350-700 nm region as seen for Mb in Fig. 1. The radiation-induced changes of metal sites are quite fast, and a composite data collection strategy (collecting data on several different crystals and combining the slices experiencing the same dose) have been established, as well as attempts to reduce the damage by adding scavengers [8, 9]. The program *RADDOSE* can be used to compute the absorbed dose by the protein crystal [59, 60]. A very powerful way of studying metalloproteins is obtained by combining both single-crystal rRaman, crystallography and microspectrophotometry [61]. We will discuss three states of Mb, where the two first cases represent undesired radiation-induced changes to the redox-states, while in the third case, the radiation-induced changes are exploited to deliver an electron resulting in generation and trapping of an otherwise unattainable intermediate by crystallography.

4. Radiation-induced resting ferric metMb

The ferric metMb is the resting state in the peroxidase reaction of Mb, and due to its ferric oxidation state it can potentially be reduced. This undesired radiation-induced change is observed for the ferric metMb state during crystallographic data collection [8, 12, 62]. Already in the 1970's Gasyna showed that ferric Mb can be one-electron reduced by ^{60}Co γ-irradiation in frozen solution at 77 K [63], and a more detailed study was performed in 2007 by Denisov *et al.* [64]. The radiation-induced reduction reduces the Fe^{III} to Fe^{II}, but at this low temperature the water that ligates to the iron is unable to move away to generate the normal ferrous deoxy [65, 66]. The reduction by ^{60}Co γ-irradiation or X-rays have led to trapping of a low-spin (S=0) Fe^{II}-H_2O/OH^- state that is unstable at room temperature [63, 65-67]. The crystal structure of the aqua ferrous low-spin state can be seen in Fig. 3A with a Fe-O bond of 2.1 Å, which is about 0.1 Å shorter

than in the high-spin ferric metMb state [12, 62]. The cryoradiolytic-induced conversion from ferric metMb to aqua/hydroxy-ferrous Mb can in crystals be followed with single-crystal microspectrophotometry as seen in Fig. 2A [68]. The reduction is characterised by the reduction of the original ferric metMb peaks at 500, 540, 580 and 635 nm, with new peaks at 525 and 567 nm as well as at 535 and 555 nm depending on the crystal and orientation (Fig. 1 and 2A), and a Soret shift from 413 to 427 nm [8, 12, 68]. With the use of an on-line microspectrophotometer, Beitlich *et al.* have estimated that the 566-7 peak reach a maximum at a dose of 2 MGy, which can fit with our findings with use of an off-line microspectrophotometer (Fig. 2A) [8, 68]. Beitlich *et al.* have in their comprehensive study further investigated the effect of wavelength, scavengers and cryo-solution on the rate of radiation-induced reduction [8]. The photoreduction was monitored in the wavelength range from 0.8 to 1.8 Å showing a maximum at 1.4 Å. Scavengers such as ascorbate yielded a decrease in photoreduction by some 20%, while introduction of glycerol as cryo agent increased the photoreduction [8]. It seems that combining the choice of wavelength, scavengers and cryo-solution with a composite data collection strategy is needed to solve the unreduced ferric metMb structure.

In frozen solutions, the low-spin ferrous intermediate relax to the normal high-spin ferrous deoxy Mb during heating [65, 66]. When we carry out a short annealing of the aqua-ferrous state in crystals it seems that it is the high-spin ferric Mb state that is regenerated and not the ferrous deoxy state (Fig. 2A; [12, 68]. The generated state must be very unstable at higher temperatures in the crystal, and the water molecule must be unable to escape so a regeneration of the ferric state is more favourable than the ferrous deoxy state with the electron possibly being taken up by the cryo-solution. This marks a difference between the cryoradiolytic reduction in solutions and crystals.

5. Radiation-induced Mb compound II

The high-valent compound I and II states have been extensively studied during the last decade. Crystal structures for HRP, Mb, P450, CCP and catalase have been published [9, 10, 12, 69-76], and an increased awareness of potential radiation-induced reduction has evolved.

Single-crystal microspectrophotometry on Mb compound II shows radiation-induced changes during crystallographic data collection (Fig. 2B) [12, 68]. The peaks at 540 and 580 as well as the shoulder peak at 595 nm decreases with increasing dose, while a new peak at 567 nm

of unknown origin appears (Fig. 2B). The structure of this radiation-induced Mb compound II has a Fe-O bond of 1.85-1.90 Å, which indicate a single-bond (Fig. 3B) [12]. The observation of a single-bond in compound II is supported by crystallographic studies on HRP, CCP and catalase [9, 10, 74]. For HRP the compound II structure was solved by a careful composite data-collection strategy to avoid radiation-induced changes [9]. A Fe-O bond distance of 1.85-1.90 Å is about 0.3 Å longer than expected for an oxoferryl (Fe^{IV}=O) species and about 0.2 Å shorter than in the radiation-induced ferric Mb structures. We have also collected datasets with shorter exposure time, and only partially radiation-induced structures as shown from single-crystal light absorption spectra [12]. These structures show similar Fe-O bond distances of 1.85-1.90, which indicates that the unaffected compound II and the radiation-induced compound II may have similar structures. Density functional theory (DFT) calculations in vacuum as well as quantum refinements (see description below) on one of the radiation-induced Mb compound II structures was performed to obtain a more detailed picture of the state with regard to oxidation state and protonation of the oxygen-atom and the distal His. The quantum refinement showed that at least in the radiation-induced Mb compound II crystal structure, the oxygen atom bound to the iron is protonated (Fe-OH) [77]. We believe, as mentioned above, that the structure of the Mb compound II and radiation-induced Mb compound II are similar, and thereby both Fe-OH states. Due to the shown protonation of the radiation-induced Mb compound II it has also been referred to as Mb intermediate H.

The compound I and II states in haemproteins have been extensively studied during the last years with theoretical methods by a number of different research groups [44, 77-84]. Several have shown that a protonated compound II state results in Fe-O bond distances in accordance with the recent crystal structures, and also proposed that the active compound II state is the protonated form [77, 80, 82, 84-87]. It is still under debate whether presence of a protonated form is general or true only for the thiolate systems with the higher proton affinity compared to His-ligated systems [7, 82, 88]. Crystal structures of compound II indicate a single-bond character, while extended X-ray absorption fine structure (EXAFS) studies still indicate a double-bond character for the His-ligated compound IIs (except for an older EXAFS study on HRP that gives a long 1.9 Å Fe-O bond), while Cys-ligated ones show a single-bond [86, 89, 90]. Mössbauer and DFT studies on CPO, P450, and catalase have shown that a protonated ferryl species Fe^{IV}-OH would have an enlargement in the quadrupole splitting parameters compared to an unprotonated ferryl

Fe^{IV}=O [91-93]. DFT-calculations determining the Mössbauer parameters for Mb indicate that the Mb compound II is unprotonated [88]. These results could then indicate that in solution, our Mb compound II should consist of an unprotonated ferryl state, while intermediate H in crystals still contains an OH^- ion as shown by quantum refinement [77]. However, as mentioned above we do not observe a shortening of the Fe-O bond in the partially radiation induced data sets, which indicates that compound II should have a relatively long Fe-O bond as well. Resonance Raman spectroscopy (rRaman) have indicated a double-bond for HRP, CCP and Mb compound II from the observation of the Fe-O mode at 797 cm^{-1} (Mb) (or at 790 at low and 804 cm^{-1} at high pH), 779 cm^{-1} (HRP) and 767 cm^{-1} for CCP compound I [88, 94-98], while both EXAFS and rRaman have indicated a single-bond for CPO compound II [86, 99]. However, we have observed a ^{18}O-sensitive Fe-O mode at 687 cm^{-1} in the pH range 5.2-8.7 for Mb compound II that could support the long Fe-O bond observed by X-ray diffraction [12, 68]. A recent nuclear resonance vibrational spectroscopy study have indicated that Mb compound II is unprotonated in solution with a Fe-O mode of 805 cm^{-1}, while Fe^{III}-OH has a mode at 556 cm^{-1} [100]. From their calculations, they suggest that the Mb^{III}-OH is a likely result from reduction of Mb^{IV}=O under intense X-ray irradiation, a state that would be indistinguishable from Mb^{IV}-OH [100]. However, both an acid and basic ferrylMb form have been observed, and from MCD it has been suggested to be the acid form that closely resembles the typical peroxidase compound II species [101-103]. Silaghi-Dumitrescu *et al.* have shown that ferrylMb has a pK_a value of 4.7 in solution, and that it is the protonated ferrylMb form that has the largest reactivity [84]. The protonated ferrylMb might be stabilised in the crystal structures even at pH values above 4.7, explaining the difference between the results from spectroscopy on solutions and crystallography on crystals. For Mb one of the main issues to be resolved is the difference between the Mb compound II in solution and crystals, and in crystals between Mb compound II and the radiation-induced Mb compound II (intermediate H).

6. Radiation-induced generation of peroxyMb.

6.1. Crystal structure

Mb compound III, which is similar to a ferrous-oxy (or ferric-superoxy) state (Scheme 1) has been generated in Mb crystals (Fig. 2C and 2D) [11]. As with the other Mb states, Mb compound III also experiences a fast one-electron reduction by the synchrotron radiation during the crystallographic data collection, and similar results have been observed for oxyMb [11, 14]. A

one-electron reduction of the compound III or oxy state leads to a peroxy intermediate that is isoelectric with compound 0.

The formation of compound III from compound II in Mb crystals can be seen by the disappearance of the 595 nm light absorption shoulder peak, resulting in only two quite sharp peaks at 540 and 580 nm (Fig. 2C). This is typical for low-temperature oxyMb spectra [104]. It has been shown that the oxyMb is quite easily one-electron reduced by ^{60}Co γ-irradiation [67, 104], as well as oxyP450, oxyHRP and oxyCPO [29, 105, 106]. Similar spectroscopic changes as observed by ^{60}Co γ-irradiation, are observed for synchrotron X-ray irradiated Mb compound III (Fig. 2C) and oxyMb [11, 14]. The Mb compound III peaks at 540 and 580 nm decrease, while a new small peak at 567 nm appears showing the formation of peroxyMb (Fig. 1 and 2C). For the peroxyMb spectrum an additional peak is observed in the Soret region at shorter wavelengths compared to the 425 nm compound III peak (Fig. 2D). This results in two peaks at 360 and 433 nm, which resemble a "hyperphorphyrin" spectrum (Fig. 2D) [107]. Similar observations in HRP and P450 with an extra peak in the Soret region have been proposed to indicate the hydroperoxy/compound 0 intermediate [107, 108].

The crystal structures of peroxyMb generated from Mb compound III (Fig 3C and 4C) and from oxyMb (Fig. 4B) were solved independently by two groups [11, 14, 68]. These two peroxyMb structures are quite similar with O-O bonds of ~1.3 Å (1.26 Å and 1.33 Å), and Fe-O distances of ~1.8-1.9 Å. The O-O bond of 1.26 Å is possibly a bit too short, and quantum refinement (see below) on this structure has resulted in an O-O bond of 1.34 Å, which is more in accordance with the peroxyMb generated from oxyMb. The structures are also very similar to the oxyMb with similar Fe-O and O-O distances as well as O-O orientation (Fig. 4A). The overall structure is also quite similar to both radiation-induced ferric Mb and radiation-induced Mb compound II structures (Fig. 3) [12].

We have collected two consecutive datasets on a Mb compound III crystal, the first one with a dose of ~3 MGy (Dataset 1), and the second one with a dose of ~10 MGy (Dataset 2) [11]. The light absorption spectrum collected after Dataset 2 shows the characteristic peroxyMb features (Fig. 2C). The structures resulting from Dataset 1 and Dataset 2 are shown in Fig. 5A and 5B, and indicate a shorter O-O bond for the primer. The trend indicates that Dataset 1 is mostly compound III (oxy) with a shorter O-O bond, while Dataset 2 is mostly peroxyMb, but the resolution is not high enough to give conclusive results, and a bond of 1.16 Å is clearly too short

for an oxy species indicating that the distance is underestimated. Unno *et al.* were able to avoid the radiation-induced reduction of oxyMb during crystallographic data collection by collecting the data with a wavelength of 0.6 Å instead of the more common ~0.9 Å [14]. They therefore obtained an unreduced oxyMb structure (Fig. 4A) and showed that it is quite similar to the peroxyMb with only a slightly shorter O-O bond of 1.25 Å [14]. For HRP compound III a composite data collection strategy was used to solve the structure (Fig. 4F) [9].

An issue to be raised is if it is the peroxyMb or the hydroperoxyMb state that has been trapped and solved with X-ray diffraction. Both optical absorption, EPR and Mössbauer spectroscopy have shown that the cryoradiolytically reduced oxyMb is a peroxyMb state, and that temperatures near 185 K are needed to induce a proton transfer resulting in hydroperoxyMb [28, 67]. The ~1.3 Å O-O bond observed in the crystal structures of peroxyMb also indicates a peroxyMb state, as a longer bond would be expected for a hydroperoxy state. For HO and P450, the peroxy state is protonated at a considerably lower temperature of ~6K and ~55 K, respectively [105, 109, 110]. The same is true for CPO where crystal structure of the cryoradiolytically reduced oxyCPO show a longer O-O bond of ~1.5 Å indicating a hydroperoxy state (Fig. 4E) [13].

Quantum refinement on peroxyMb generated from compound III shows that the major spin density resides on the O-O (Fig. 6), indicating a Fe^{II}-O-O^{-}, superoxy state (see below) [11]. Similar results with the unpaired electron residing on the O-O have been obtained with QM/MM (Quantum Mechanical / Molecular Mechanics) calculations on peroxyMb generated from oxyMb [14]. However, EPR and Mössbauer spectroscopy indicates the Fe^{III} peroxy state [67].

6.2. Quantum mechanical calculations

6.2.1. Vacuum calculations

Further information about these intermediates can be gained from quantum mechanical (QM) calculations. The advantage of such calculations is the exact knowledge of the nature of the complex being studied and the absence of experimental limitations (e.g. that the complex is very short-lived). Therefore, they can be used to obtain information of the ideal structure of possible complexes, which can be used to interpret the experimental results. On they other hand, the QM calculations involve some approximation and sometimes ignore the effect of the surrounding protein. Therefore, they have a limited, but quite good, accuracy. For example, normal bond lengths are typically correct to within 0.02 Å and metal–ligand bond lengths to within 0.05 Å

[111, 112]. This is actually better than in low- and medium-resolution crystal structures, for which the average error is 0.1 Å and errors of up to ~0.3 Å are frequently observed [113-115].

To get a feeling of the expected structure of the oxy, peroxy, and hydroperoxy complexes of haem, we first consider the results of vacuum QM calculations. Isolated complexes have been studied by many groups [44, 116], but we will also consider the effect of the distal His residue, which may form a hydrogen bond to the iron ligand, thereby changing the Fe–O bond length by up to 0.1 Å [77]. The distal His is a versatile group that may function both as a hydrogen-bond acceptor and donor, and in the latter case, it may be both neutral or positively charged. We call these three configurations HID, HIE, and HIP in the following (cf. Fig. 7). Thus, an oxy and peroxy group can be combined with the HIE and HIP forms, whereas the hydroperoxy ligand can be combined with all three configurations, giving rise to seven different complexes, the vacuum structures of which are described in Table 1.

It can be seen that the structures of the seven complexes are quite similar: The Fe–N_{Por} distances are ~2.02 Å for all complexes and the Fe–N_{His} distances are 2.03–2.07 Å. Even for the Fe–O distance, the variation is small, 1.78–1.87 Å, with the shortest bond for the hydroperoxide complexes and the longest one for the peroxy complexes. The variation the O–O bond is slightly larger, it is 1.30–1.33 Å in the oxy complexes, 1.34–1.38 Å for the peroxy complexes, and 1.43–1.54 Å for the hydroperoxy complexes. This reflects the electronic structure of the complexes. The two last columns in Table 1 show the spin density on the iron ion and the (H)O_2 ligand (the other parts of the complexes have less than 0.07 *e* spin). It can be seen that the oxy complexes have almost one unpaired electron (~0.75 *e*) on the O_2 group, indicating that it actually is a superoxide anion ($O_2^{-\bullet}$, which has an ideal bond length of 1.33 Å; that of free O_2 is 1.21 Å [117]). A nearly equal amount of opposite spin is present on the Fe ion, indicating that it is in the low-spin Fe^{III} state, and the two spins couple antiferromagnetically to an open-shell singlet. This is the normal electronic structure observed for O_2–haem complexes [118].

The peroxy complex also has significant spin on O_2 (0.6–0.8 *e*), indicating that it still contains a superoxide anion (cf. Fig. 6). The spin on iron has decreased and changed to the same sign as the O_2 ligand, indicating that it has been reduced to Fe^{II}. However, when the ligand is protonated, its spin decreases and the O–O bond length increases, indicating a true hydroperoxide ion (HO_2^- with an ideal bond length of ~1.49 Å [117]. At the same time the spin on Fe approaches 1, i.e. low-spin Fe^{III}.

An even larger variation, 2.46–2.94 Å, is found in the distance between the distal O atom and the N atom of the distal His residue. The shorter distances (2.46–2.62 Å) are obtained when the distal His is positively charged (HIP state). The peroxy complexes give a ~0.2 Å shorter distance than the oxy complexes, and the HID state of the hydroperoxide complexes (for which HO_2 is the donor) gives a 0.15 Å shorter distance than the HIE state. The hydroperoxy–HID and HIE complexes have the same atoms and number of electrons, and are therefore energetically comparable. From Table 1, it can be seen that they differ by only 2 kJ/mol in energy (which can easily be changed by interactions with surrounding groups in the protein). On the other hand, the peroxy–HIP complex, which can be obtained from the hydroperoxy–HID by a transfer of the proton from HO_2 to HID, is 58 kJ/mol higher in energy, and therefore less likely to be observed.

6.2.2. Quantum refinement

Considering the excellent geometric accuracy of theoretical calculations [111, 112], theoretical structures can be used to interpret crystal structures. In fact, this is already done in nearly all crystal structures, in which a molecular mechanics (MM) force field is used to supplement the crystallographic raw data and ensure that bond lengths and angles are chemically reasonable [119]. However, for metal complexes, standard MM methods perform poorly, and no general force fields exist. Therefore, the accuracy of metal–ligand bond lengths is typically worse than for other bonds in the protein.

This can be cured by using QM data instead. We have developed a method in which the MM force field is replaced by QM calculations in the crystallographic refinement procedure for a small, but interesting, part of the protein, e.g. a metal site [120] and improve the crystal structures locally [121]: By re-refining a 1.7-Å resolution structure of cytochrome c_{553} by our method, we could reduce the errors in the iron-ligand distances, compared to a 0.97-Å structure of the same protein [122], from 0.32, 0.12, and 0.03–0.09 Å to 0.02, 0.04, and 0–0.01 Å for the Fe–N_{His}, Fe–S_{Met}, and Fe–N_{Por} bonds, respectively. Moreover, we have shown that the method can be used to determine the protonation state of metal-bound solvent molecules [123]: By re-refining two structures of alcohol dehydrogenase with ligands in two different protonation states, we showed that in the first [124] an alkoxide was bound to the catalytic zinc ion, whereas in the second [125] a neutral water molecule was bound, both in agreement with kinetically determined pKa values [126].

We have tested this approach also for the crystal structure of peroxy Mb by refining the

crystal structure using the seven possible cases in Table 1 for the QM system [11]. The results are gathered in Table 2. We use four different criteria to deduce which of the seven QM systems fit the crystallographic raw data best: the R_{free} factor, the residue (real-space) R factor, the difference in the Fe–ligand distances between the quantum refined and vacuum structures (Δr_{QM}), and the energy difference of the QM system between the quantum refined and vacuum structures (ΔE_{QM1}). Unfortunately, the four criteria give different results: The R_{free} factor is lowest for the hydroperoxy–HIP complex, the residue R factor and Δr_{QM} are lowest for the oxy–HIE complex, whereas ΔE_{QM1} is lowest for the hydroperoxy–HID complex.

The reason for this is the small geometric difference between the various complexes and therefore the small difference in the quality criteria between them. As we saw in Table 1, the only really significant difference between the various complexes is in the distance between the distal O atom and N in the distal His residue. By looking at the electron density maps (which are strongly correlated to the residue R factor), it can be seen that the short O–N distances of the HIP states are not in accordance with the electron density. Considering the experimental conditions (we start from oxy complex and reduce it during data collection, but the temperature is too low to allow for protonation), the peroxy–HIE complex, possibly partly mixed up with some oxy–HIE, seems to be the most plausible interpretation of the structure. Quite satisfactorily, this quantum-refined structure is very similar to the original crystal structure (which did not use any restraints around the Fe ion): The largest difference is 0.08 Å for the O–O distance. Considering the expected accuracy of the two methods, the quantum-refined results should be slightly more reliable.

7. Breaking of oxygen-oxygen bond.

Cryoradiolytical reduction of oxyMb generates peroxyMb, and it has been shown by EPR spectroscopy that an annealing to temperatures 190-200 K generates the hydroperoxyMb [127-129]. Mössbauer studies with annealing to 195 K have, however, resulted in the breaking of the O-O bond forming Mb compound II [67]. This is different from oxyHO that is cryoradiolytically reduced to hydroperoxyHO at 77 K (also with amounts of ferrylHO), which by annealing propagates to the α-meso-hydroxyhemin HO product [67].

Schlichting *et al*. have for P450 previously taken advantage of the effect observed above for HO [72]. They have collected a dataset on the oxyP450 with a wavelength of 0.91 Å (Fig. 5D),

and then, by increasing the wavelength to 1.5 Å, been able to break the O-O bond at 100 K and reduce the state to compound I (Fig. 5E) [72]. An annealing of the putative compound I generates the 5-exo-hydroxy-camphor product. A reduction of oxyP450 to peroxy/hydroperoxyP450 in crystal structures have recently been observed during data collection [8].

For Mb a short annealing of 1 sec. of the peroxyMb crystal (already collected Dataset 1 and 2 on, see above) resulted in the formation of Mb compound II (Fig. 2C, after annealing) [11]. The characteristic shoulder at 595 nm can be seen, but it has a relative lower intensity than normal, so the conversion might not be complete. The structure of the dataset collected on this state (Dataset 3) can be seen in Fig. 5C, and will during data collection result in the radiation-induced compound II as indicated by the light absorption spectra (Fig. 2C). From Fig. 5B and 5C it is clearly seen by the electron density difference maps that the molecular oxygen has changed into a single oxygen atom. The Fe-O distance of the radiation-induced compound II is, however, 0.1 Å longer than expected for this state by comparing it to the previously published high-resolution structure (Fig. 3B) [12].

These results show that compound III can be cryoradiolytically reduced to a peroxyMb state that is analogous to the proposed compound 0 precursor in the reaction with hydrogen peroxide. The state propagates to compound II upon heating. The hydroperoxy state is an important intermediate in the peroxidase reaction cycle, as well as important for the oxygen-activation of P450 monooxygenases. In Mb, annealing is needed to break the O-O bond, while in P450 the breaking occurs at 100 K with the use of a wavelength of 1.5 Å.

8. Summary.

The structural studies on Mb have shown that most oxidised states of Mb experience some radiation-induced changes during crystallographic data collection from interactions with X-rays, and similar observations have been made for other haem proteins. The ferric metMb, Mb compound II and Mb compound III / oxyMb experiences undesired X-ray radiation-induced changes/reductions [11, 12, 14, 68]. These reductions occur at doses well below the classical Henderson limit of 20 MGy [52]. The unreduced oxyMb structure have, however, been obtained through the use of short 0.6 Å wavelength, and for HRP unreduced states have been obtained through the use of a composite data collection strategy [9, 14]. Additionally to the use of shorter wavelength and composite data collection strategies, the application of scavengers and avoidance

of glycerol in the cryo-solution have also shown decreased reduction of ferric metMb [8]. For the most easily reduced states a combination of different techniques may be needed. To be able to characterise these states further probably a combination of both X-ray diffraction and single-crystal microspectrophotometry, rRaman and EPR studies are required.

The X-ray induced reduction during crystallographic data collection can also be used to add an electron to a state at low temperatures, generating intermediates that are otherwise unattainable. For Mb the crystal structure of peroxyMb has been generated in this way from both oxyMb and Mb compound III [11, 14]. An annealing of the peroxyMb has shown that the oxygen-oxygen bond is broken in the crystal resulting in Mb compound II. This shows a way of trapping such intermediates, and that the peroxy/hydroperoxy state is an important intermediate in Mb peroxidase reaction cycle.

9. Acknowledgements

Our investigation has been supported by funding from the Norwegian Research Council: grant 177661/V30 (to K.K.A) and grant 138370/V30 (Synchrotron related research in the Oslo-region, SYGOR), by funding from the Swedish Research Council and by computer resources of LUNARC at Lund University. The teams at the Swiss-Norwegian Beam Line (BM01) and the Cryo-Bench at ESRF are thanked for their valuable help.

REFERENCES:

[1] K.N. Degtyarenko, A.C.T. North, J.B.C. Findlay, *Protein Engng* **1997**, *10*, 183.

[2] K.R. Rodgers, *Curr. Opin. Chem. Biol* **1999**, *3*, 158.

[3] Y. Watanabe, H. Nakajima, T. Ueno, *Acc. Chem. Res.* **2007**, *40*, 554.

[4] P. Nicholls, I. Fita, P.C. Loewen, *Adv. Inorg. Chem.* **2001**, *51*, 51.

[5] N.C. Veitch, A.T. Smith, *Adv. Inorg. Chem.* **2001**, *51*, 107.

[6] T.L. Poulos, *Phil. Trans. R. Soc. A* **2005**, *363*, 793.

[7] H.-P. Hersleth, U. Ryde, P. Rydberg, C.H. Görbitz, K.K. Andersson, *J. Inorg. Biochem.* **2006**, *100*, 460.

[8] T. Beitlich, K. Kühnel, C. Schulze-Briese, R.L. Shoeman, I. Schlichting, *J. Synchrotron Rad.* **2007**, *14*, 11.

[9] G.I. Berglund, G.H. Carlsson, A.T. Smith, H. Szöke, A. Henriksen, J. Hajdu, *Nature* **2002**, *417*, 463.

[10] C.A. Bonagura, B. Bhaskar, H. Shimizu, H. Li, M. Sundaramoorthy, D. McRee, D.B. Goodin, T.L. Poulos, *Biochemistry* **2003**, *42*, 5600.

[11] H.-P. Hersleth, Y.-W. Hsiao, U. Ryde, C.H. Görbitz, K.K. Andersson, *Biochem. J.* **2008**, In press. doi:10.1042/BJ20070921.

[12] H.-P. Hersleth, T. Uchida, Å.K. Røhr, T. Teschner, V. Schünemann, T. Kitagawa, A.X. Trautwein, C.H. Görbitz, K.K. Andersson, *J. Biol. Chem.* **2007**, *282*, 23372.

[13] K. Kühnel, E. Derat, J. Terner, S. Shaik, I. Schlichting, *Proc. Natl. Acad. Sci. USA* **2007**, *104*, 99.

[14] M. Unno, H. Chen, S. Kusama, S. Shaik, M. Ikeda-Saito, *J. Am. Chem. Soc.* **2007**, *129*, 13394.

[15] H. Günther, *Virchow's Arch. path. Anat.* **1921**, *230*, 146.

[16] G.A. Millikan, *Proc. R. Soc. Lond. B.* **1937**, *123*, 218.

[17] B.A. Wittenberg, J.B. Wittenberg, *Annu. Rev. Physiol.* **1989**, *51*, 857.

[18] G.N. Phillips Jr. in (Messerschmidt, A., Huber, R., Poulos, T. and Wieghardt, K., eds.) Hanbook of Metalloproteins, John Wiley & Son, Ltd, Chichester 2001, p. 5.

[19] H. Frauenfelder, B.H. McMahon, R.H. Austin, K. Chu, J.T. Grooves, *Proc. Natl. Acad. Sci. USA* **2001**, *98*, 2370.

[20] D.J. Garry, S.B. Kanatous, P.P.A. Mammen, *Trends Cardiovasc. Med.* **2003**, *13*, 111.

[21] M. Brunori, *Trends Biochem. Sci.* **2001**, *26*, 209.

[22] A.I. Alayash, R.P. Patel, R.E. Cashon, *Antioxid. Redox. Signal.* **2001**, *3*, 313.

[23] M.T. Wilson, B.J. Reeder, *Exp. Physiol.* **2008**, *93*, 128.

[24] B.J. Reeder, M.T. Wilson, *Curr. Med. Chem.* **2005**, *12*, 2741.

[25] D. Keilin, E.F. Hartree, *Nature* **1950**, *166*, 513.

[26] P. George, D.H. Irvine, *Nature* **1951**, *168*, 164.

[27] P. George, D.H. Irvine, *Biochem. J.* **1952**, *52*, 511.

[28] M. Ibrahim, I.G. Denisov, T.M. Makris, J.R. Kincaid, S.G. Sligar, *J. Am. Chem. Soc.* **2003**, *125*, 13714.

[29] I.G. Denisov, T.M. Makris, S.G. Sligar, *J. Biol. Chem.* **2002**, *277*, 42706.

[30] M. Ibrahim, J.R. Kincaid, *J. Porphyrins Phthalocyanines* **2004**, *8*, 215.

[31] T. Egawa, H. Shimada, Y. Ishimura, *J. Biol. Chem.* **2000**, *275*, 34858.

[32] T. Egawa, S. Yoshioka, S. Takahashi, H. Hori, S. Nagano, H. Shimada, K. Ishimori, I. Morishima, M. Suematsu, Y. Ishimura, *J. Biol. Chem.* **2003**, *278*, 41597.

[33] T. Matsui, S.-i. Ozaki, E. Liong, G.N. Phillips, Jr., Y. Watanabe, *J. Biol. Chem.* **1999**, *274*, 2838.

[34] C.E. Cooper, M. Jurd, P. Nicholls, M.M. Wankasi, D.A. Svistunenko, B.J. Reeder, M.T. Wilson, *Dalton Trans.* **2005**, 3483.

[35] T.L. Poulos, J. Kraut, *J. Biol. Chem.* **1980**, *255*, 8199.

[36] M. Sono, M.P. Roach, E.D. Coulter, J.H. Dawson, *Chem. Rev.* **1996**, *96*, 2841.

[37] J. Everse, *Free Rad. Biol. Med.* **1998**, *24*, 1338.

[38] N.K. King, M.E. Winfield, *J. Biol. Chem.* **1963**, *238*, 1520.

[39] C. Guilivi, E. Cadenas, *Meth. Enzymol.* **1994**, *233*, 189.

[40] Y. Watanabe, T. Ueno, *Bull. Chem. Soc. Jpn.* **2003**, *76*, 1309.

[41] S.-i. Ozaki, T. Matsui, Y. Watanabe, *J. Am. Chem. Soc.* **1997**, *119*, 6666.

[42] S.-i. Ozaki, T. Matsui, M.P. Roach, Y. Watanabe, *Coord. Chem. Rev.* **2000**, *198*, 39.

[43] T.L. Poulos, *Biochem. Biophys. Res. Comm.* **2005**, *338*, 337.

[44] P. Rydberg, E. Sigfridsson, U. Ryde, *J. Biol. Inorg. Chem.* **2004**, *9*, 203.

[45] D. Keilin, T. Mann, *Proc. R. Soc. Lond. B.* **1937**, *122*, 119.

[46] P. George, *J. Biol. Chem.* **1953**, *201*, 427.

[47] B. Chance, J. Higgins, *Arch. Biochem. Biophys.* **1952**, *41*, 432.

[48] E.F. Garman, R.L. Owen, *Acta Cryst. D* **2006**, *62*, 32.

[49] R.B.G. Ravelli, E.F. Garman, *Curr. Opin. Chem. Biol* **2006**, *16*, 624.

[50] C.M. Wilmot, T. Sjögren, G.H. Carlsson, G.I. Berglund, J. Hajdu, *Meth. Enzymol.* **2002**, *353*, 301.

[51] C.C.F. Blake, D.C. Phillips. in Symposium on the Biological Effects of Ionizing Radiation at the Molecular Level., International Atom Energy Agency, Vienna 1962.

[52] R. Henderson, *Proc. R. Soc. Lond. B.* **1990**, *241*, 6.

[53] R.L. Owen, E. Rudiño-Piñera, E.F. Garman, *Proc. Natl. Acad. Sci. USA* **2006**, *103*, 4912.

[54] M. Weik, R.B.G. Ravelli, G. Kryger, S. McSweeney, M.L. Raves, M. Harel, P. Gros, I. Silman, J. Kroon, J.L. Sussman, *Proc. Natl. Acad. Sci. USA* **2000**, *97*, 623.

[55] J. Yano, J. Kern, K.-D. Irrgang, M.J. Latimer, U. Bergmann, P. Glatzel, Y. Pushkar, J. Biesiadka, B. Loll, K. Sauer, J. Messinger, A. Zouni, V.K. Yachandra, *Proc. Natl. Acad. Sci. USA* **2005**, *102*, 12047.

[56] O. Carugo, K.D. Carugo, *Trends Biochem. Sci.* **2005**, *30*, 213.

[57] V. Srajer, Z. Ren, T.-Y. Teng, M. Schmidt, T. Ursby, D. Bourgeois, C. Pradervand, W. Schildkamp, M. Wulff, K. Moffat, *Biochemistry* **2001**, *40*, 13802.

[58] D. Bourgeois, X. Vernede, V. Adam, E. Fioravanti, T. Ursby, *J. Appl. Cryst.* **2002**, *35*, 319.

[59] J.W. Murray, R.B.G. Ravelli, E.F. Garman, *J. Appl. Cryst.* **2004**, *37*, 513.

[60] J.W. Murray, E. Rudiño-Piñera, R.L. Owen, M. Grininger, R.B.G. Ravelli, E.F. Garman, *J. Synchrotron Rad.* **2005**, *12*, 268.

[61] G. Katona, P. Carpentier, V. Niviere, P. Amara, V. Adam, J. Ohana, N. Tsanov, D. Bourgeois, *Science* **2007**, *316*, 449.

[62] N. Engler, A. Ostermann, A. Gassmann, D.C. Lamb, V.E. Prusakov, J. Schott, R. Schweitzer-Stenner, F.G. Parak, *Biophys. J.* **2000**, *78*, 2081.

[63] Z. Gasyna, *Biochim. Biophys. Acta* **1979**, *577*, 207.

[64] I.G. Denisov, D.C. Victoria, S.G. Sligar, *Rad. Phys. Chem.* **2007**, *76*, 714.

[65] D.C. Lamb, A. Ostermann, V.E. Prusakov, F.G. Parak, *Eur. Biophys. J.* **1998**, *27*, 113.

[66] V.E. Prusakov, J. Steyer, F.G. Parak, *Biophys. J.* **1995**, *68*, 2524.

[67] R. Garcia-Serres, R.M. Davydov, T. Matsui, M. Ikeda-Saito, B.M. Hoffman, B.H. Huynh, *J. Am. Chem. Soc.* **2007**, *129*, 1402.

[68] H.-P. Hersleth, A. Varnier, E. Harbitz, Å.K. Røhr, P.P. Schmidt, M. Sørlie, F.H. Cederkvist, S. Marchal, A.C.F. Gorren, B. Mayer, T. Uchida, V. Schünemann, T. Kitagawa, A.X. Trautwein, T. Shimizu, R. Lange, C.H. Görbitz, K.K. Andersson, *Inorg. Chim. Acta* **2008**, In press. doi:10.1016/j.ica.2007.09.045.

[69] S.L. Edwards, N.h. Xuong, R.C. Hamlin, J. Kraut, *Biochemistry* **1987**, *26*, 1503.

[70] V. Fülöp, R.P. Phizackerley, S.M. Soltis, I.J. Clifton, S. Watatsuki, J. Erman, J. Hajdu, S.L. Edwards, *Structure* **1994**, *2*, 201.

[71] P. Gouet, H.-M. Jouve, P.A. Williams, I. Andersson, P. Andreoletti, L. Nussaume, J. Hajdu, *Nat. Struct. Biol.* **1996**, *3*, 951.

[72] I. Schlichting, J. Berendzen, K. Chu, A.M. Stock, S.A. Maves, D.E. Benson, R.M. Sweet, D. Ringe, G.A. Petsko, S.G. Sligar, *Science* **2000**, *287*, 1615.

[73] H.-P. Hersleth, B. Dalhus, C.H. Görbitz, K.K. Andersson, *J. Biol. Inorg. Chem.* **2002**, *7*, 299.

[74] G.N. Murshudov, A.I. Grebenko, J.A. Brannigan, A.A. Antson, V.V. Barynin, G.G. Dodson, Z. Dauter, K.S. Wilson, W.R. Melik-Adamyan, *Acta Cryst. D* **2002**, *58*, 1972.

[75] P. Andreoletti, A. Pernoud, G. Sainz, P. Gouet, H.-M. Jouve, *Acta Cryst. D* **2003**, *59*, 2163.

[76] M. Alfonso-Prieto, A. Borovik, X. Carpena, G. Murshudov, W. Melik-Adamyan, I. Fita, C. Rovira, P.C. Loewen, *J. Am. Chem. Soc.* **2007**, *129*, 4193.

[77] K. Nilsson, H.-P. Hersleth, T.H. Rod, K.K. Andersson, U. Ryde, *Biophys. J.* **2004**, *87*, 3437.

[78] A. Ghosh, E. Steene, *J. Inorg. Biochem.* **2002**, *91*, 423.

[79] M.T. Green, *J. Am. Chem. Soc.* **2000**, *122*, 9495.

[80] C. Rovira, I. Fita, *J. Phys. Chem. B* **2003**, *107*, 5300.

[81] J.C. Schöneboom, F. Neese, W. Thiel, *J. Am. Chem. Soc.* **2005**, *127*, 5840.

[82] R. Silaghi-Dumitrescu, *J. Biol. Inorg. Chem.* **2004**, *9*, 471.

[83] E. Derat, S. Shaik, *J. Am. Chem. Soc.* **2006**, *128*, 8185.

[84] R. Silaghi-Dumitrescu, B.J. Reeder, P. Nicholls, C.E. Cooper, M.T. Wilson, *Biochem. J.* **2007**, *403*, 391.

[85] J. Conradie, I. Wasbotten, A. Ghosh, *J. Inorg. Biochem.* **2006**, *100*, 502.

[86] M.T. Green, J.H. Dawson, H.B. Gray, *Science* **2004**, *304*, 1653.

[87] C. Rovira, *Chemphyschem.* **2005**, *6*, 1820.

[88] R.K. Behan, M.T. Green, *J. Inorg. Biochem.* **2006**, *100*, 448.

[89] K.L. Stone, R.K. Behan, M.T. Green, *Proc. Natl. Acad. Sci. USA* **2005**, *102*, 16563.

[90] B. Chance, L. Powers, Y. Ching, T.L. Poulos, G.R. Schonbaum, I. Yamazaki, K.G. Paul, *Arch. Biochem. Biophys.* **1984**, *235*, 596.

[91] R.K. Behan, L.M. Hoffart, K.L. Stone, C. Krebs, M.T. Green, *J. Am. Chem. Soc.* **2006**, *128*, 11471.

[92] O. Horner, J.-L. Oddou, J.-M. Mouesca, H.-M. Jouve, *J. Inorg. Biochem.* **2006**, *100*, 447.

[93] K.L. Stone, L.M. Hoffart, R.K. Behan, C. Krebs, M.T. Green, *J. Am. Chem. Soc.* **2006**, *128*, 6147.

[94] S. Hashimoto, J. Teraoka, T. Inubushi, T. Yonetani, T. Kitagawa, *J. Biol. Chem.* **1986**, *261*, 11110.

[95] C.M. Reczek, A.J. Sitter, J. Terner, *J. Mol. Struct.* **1989**, *214*, 27.

[96] A.J. Sitter, C.M. Reczek, J. Terner, *Biochim. Biophys. Acta* **1985**, *828*, 229.

[97] J. Terner, V. Palaniappan, A. Gold, R. Weiss, M.M. Fitzgerald, A.M. Sullivan, C.M. Hosten, *J. Inorg. Biochem.* **2006**, *100*, 480.

[98] J. Terner, A.J. Sitter, C.M. Reczek, *Biochim. Biophys. Acta* **1985**, *828*, 73.

[99] K.L. Stone, R.K. Behan, M.T. Green, *Proc. Natl. Acad. Sci. USA* **2006**, *103*, 12307.

[100] W. Zeng, A. Barabanschikov, Y. Zhang, J. Zhao, W. Sturhahn, E.E. Alp, J.T. Sage, *J. Am. Chem. Soc.* **2008**, In press. DOI: 10.1021/ja077823+.

[101] N. Foote, P.M.A. Gadsby, C. Greenwood, A.J. Thomson, *Biochem. J.* **1989**, *261*, 515.

[102] N.K. King, M.E. Winfield, *Aust. J. Biol. Sci.* **1966**, *19*, 211.

[103] J.B. Wittenberg, *J. Biol. Chem.* **1978**, *253*, 5694.

[104] Z. Gasyna, *FEBS Lett.* **1979**, *106*, 213.

[105] R. Davydov, I.D.G. Macdonald, T.M. Makris, S.G. Sligar, B.M. Hoffman, *J. Am. Chem. Soc.* **1999**, *121*, 10654.

[106] I.G. Denisov, J.H. Dawson, L.P. Hager, S.G. Sligar, *Biochem. Biophys. Res. Comm.* **2007**, *363*, 954.

[107] H.K. Baek, H.E. Van Wart, *Biochemistry* **1989**, *28*, 5714.

[108] I.G. Denisov, T.M. Makris, S.G. Sligar, *J. Biol. Chem.* **2001**, *276*, 11648.

[109] R. Davydov, T.M. Makris, V. Kofman, D.E. Werst, S.G. Sligar, B.M. Hoffman, *J. Am. Chem. Soc.* **2001**, *123*, 1403.

[110] I.G. Denisov, M. Ikeda-Saito, T. Yoshida, S.G. Sligar, *FEBS Lett.* **2002**, *532*, 203.

[111] F. Neese, *J. Biol. Inorg. Chem.* **2006**, *11*, 702.

[112] U. Ryde, *Dalton Trans.* **2007**, 607.

[113] D.W.J. Cruickshank, *Acta Cryst. D* **1999**, *55*, 583.

[114] B.A. Fields, H.H. Bartsch, H.D. Bartunik, F. Cordes, J.M. Guss, H.C. Freeman, *Acta Cryst. D* **1994**, *50*, 709.

[115] K. Nilsson, D. Lecerof, E. Sigfridsson, U. Ryde, *Acta Cryst. D* **2003**, *59*, 274.

[116] S. Shaik, D. Kumar, S.P. de Visser, A. Altun, W. Thiel, *Chem. Rev.* **2005**, *105*, 2279.

[117] S.J. Lippard, J.M. Berg, Principles of Bioinorganic Chemistry, University Science Books, p. 287, Mill Valley, USA, 1994.

[118] K.P. Jensen, B.O. Roos, U. Ryde, *J. Inorg. Biochem.* **2005**, *99*, 45.

[119] G.J. Kleywegt, T.A. Jones, *Meth. Enzymol.* **1997**, *277*, 208.

[120] U. Ryde, L. Olsen, K. Nilsson, *J. Comp. Chem.* **2002**, *23*, 1058.

[121] U. Ryde, K. Nilsson, *J. Am. Chem. Soc.* **2003**, *125*, 14232.

[122] S. Benini, A. González, W.R. Rypniewski, K.S. Wilson, J.J. Van Beeumen, S. Ciurli, *Biochemistry* **2000**, *39*, 13115.

[123] K. Nilsson, U. Ryde, *J. Inorg. Biochem.* **2004**, *98*, 1539.

[124] B.J. Bahnson, T.D. Colby, J.K. Chin, B.M. Goldstein, J.P. Klinman, *Proc. Natl. Acad. Sci. USA* **1997**, *94*, 12797.

[125] J.K. Rubach, S. Ramaswamy, B.V. Plapp, *Biochemistry* **2001**, *40*, 12686.

[126] G. Pettersson, *CRC Crit. Rev. Biochem.* **1987**, *21*, 349.

[127] R. Kappl, M. Höhn-Berlage, J. Hüttermann, N. Bartlett, M.C.R. Symons, *Biochim. Biophys. Acta* **1985**, *827*, 327.

[128] R. Davydov, S. Chemerisov, D.E. Werst, T. Rajh, T. Matsui, M. Ikeda-Saito, B.M. Hoffman, *J. Am. Chem. Soc.* **2004**, *126*, 15960.

[129] W. Leibl, W. Nitschke, J. Huttermann, *Biochim. Biophys. Acta* **1986**, *870*, 20.

[130] G.J. Kleywegt, M.R. Harris, J.Y. Zou, T.C. Taylor, A. Wählby, T.A. Jones, *Acta Cryst. D* **2004**, *60*, 2240.

SCHEME 1

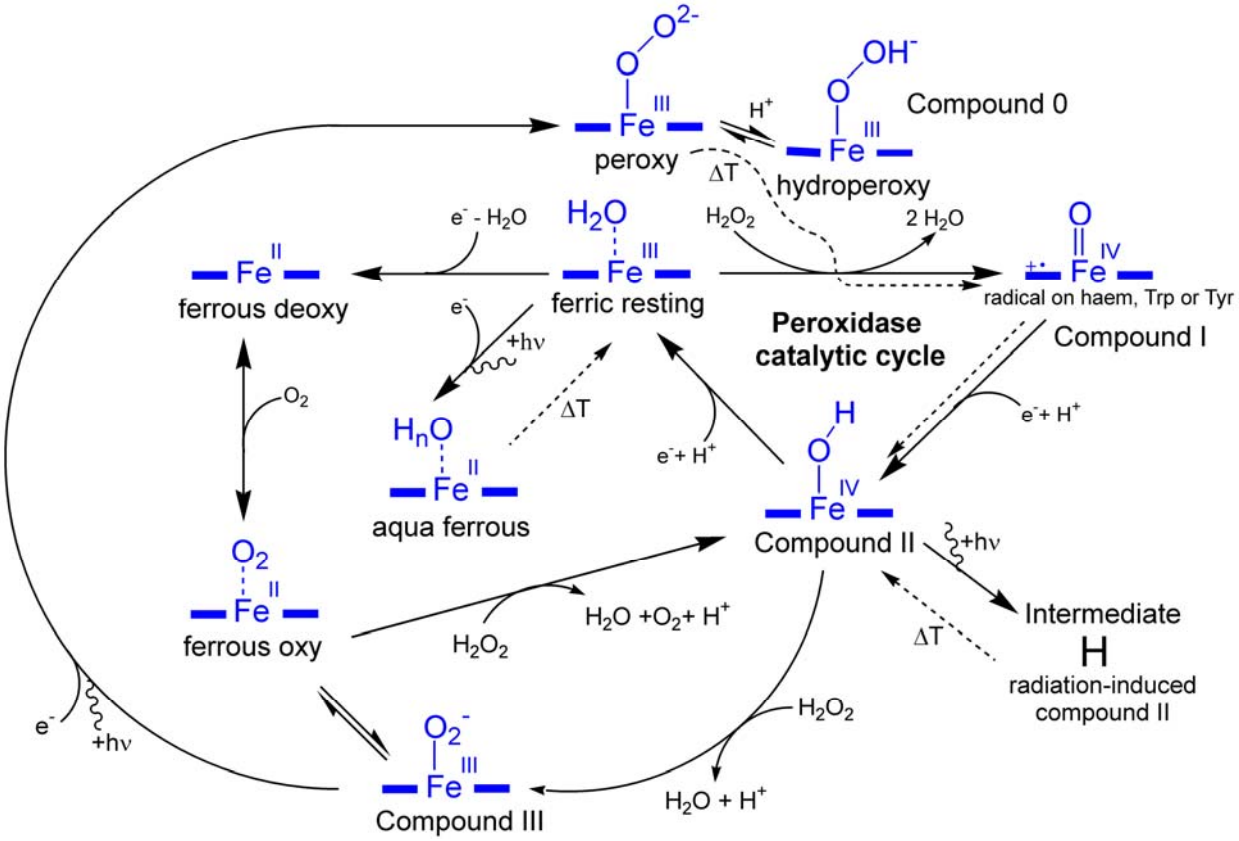
Compound 0
peroxy
hydroperoxy
ferrous deoxy
ferric resting
radical on haem, Trp or Tyr
Compound I
Peroxidase
catalytic cycle
aqua ferrous
Compound II
ferrous oxy
Intermediate
H
radiation-induced
compound II
Compound III

Table 1 – Vacuum structures of the seven possible states of the oxy, peroxy, and hydroperoxy complexes with a model of the distal His residue. Distances are in Å. ΔE is the energy difference in kJ/mole between the three indicated states (which have the same number of atoms and electrons). ρ(Fe) and $\rho(O_2)$ are the spin density on the Fe or $(H)O_2$ ligand, respectively.

		$Fe–N_{Por}$	$Fe–N_{His}$	Fe–O	O–O	O–N	ΔE	ρ(Fe)	$\rho(O_2)$
Oxy	HIE	2.00–2.03	2.07	1.81	1.30	2.94		0.78	-0.75
	HIP	1.99–2.03	2.03	1.81	1.33	2.58		0.73	-0.72
Peroxy	HIE	2.00–2.02	2.07	1.87	1.34	2.74		0.16	0.85
	HIP	1.99–2.04	2.05	1.83	1.38	2.46	58.0	0.45	0.63
Hydroperoxy	HID	2.00–2.03	2.04	1.80	1.43	2.77	0.0	0.63	0.44
	HIE	2.00–2.05	2.05	1.79	1.47	2.92	1.9	0.79	0.27
	HIP	2.00–2.03	2.03	1.78	1.54	2.62		0.87	0.18

Table 2 – Results of the quantum refinements. Residue *R* is the residue (real-space) *R* factor. Δr_{QM} is the difference in the six Fe–ligand bond lengths between the quantum refinements and QM vacuum optimizations. Likewise, ΔE_{QM1} is the energy difference (in kJ/mol) of the quantum system optimized in vacuum or with quantum refinement in the protein.

		Distances (Å)					R_{free}	Residue	Δr_{QM}	ΔE_{QM1}
		Fe–N_{Por}	Fe–N_{His}	Fe–O	O–O	O–N		*R*	(Å)	(kJ/mol)
Oxy	HIE	2.01–2.03	2.08	1.80	1.30	2.78	0.20027	0.074	5.4	32.9
	HIP	2.01–2.02	2.07	1.80	1.33	2.59	0.19998	0.089	10.1	30.7
Peroxy	HIE	2.01–2.03	2.08	1.84	1.34	2.69	0.20006	0.076	6.8	32.1
	HIP	2.00–2.03	2.08	1.83	1.38	2.46	0.19966	0.094	9.6	30.7
Hydroperoxy	HID	2.01–2.03	2.08	1.79	1.43	2.69	0.19978	0.082	8.3	29.3
	HIE	2.01–2.04	2.08	1.78	1.50	2.80	0.19986	0.085	6.6	41.6
	HIP	2.01–2.03	2.08	1.77	1.55	2.63	0.19960	0.097	8.2	35.2
Crystal [11]		2.03–2.04	2.09	1.84	1.26	2.74	0.175	0.147		

Figure 1 - Single crystal-light absorption spectra of ferrous deoxy Mb, aqua ferrous Mb (two spectra), ferric Mb, peroxyMb, Mb compound III, Mb compound II and Mb intermediate H at 110 K. The X-ray induced states are coloured in dark red, while the others in dark blue.

Figure 2 - Single crystal-light absorption spectra of ferric metMb, Mb compound II and Mb compound III during crystallographic data collection. The spectra of the states before X-ray exposure are coloured in dark blue, after X-ray exposure in dark read, and after annealing in dark green. **A**: Build up of aqua ferrous Mb from ferric Mb during increased X-ray dose, and regeneration of ferric metMb after annealing. The 1.0x dose has been estimated to be ~0.2 MGy by the use of RADDOSE. **B**: The conversion of compound II into intermediate H during data collection, and regeneration of compound II after annealing. **C**: Monitoring the changes experiences by the crystal subjected to collection of Datasets 1, 2 and 3. The crystal shows conversion from compound II to compound III after longer hydrogen peroxide soaking, and reduction to peroxyMb during data collection. Annealing of peroxyMb leads to generation of Mb compound II, which convert to intermediate H during data collection and regenerates compound II after annealing. **D**: Spectra of the Mb compound III crystal in C before Dataset 1 and after Dataset 2 are shown with extension to the Soret region

Figure 3 - The Crystal structures of the haem regions shown with the electron density 2Fo-Fc map (contoured at 1σ in golden), the final Fo-Fc map (at +3σ in green and at -3σ in red) and difference Fo-Fc map with the peroxy/hydroxy atoms and extra water molecule omitted for map calculation (at 5σ in blue). **A**: aqua ferrous Mb (resolution 1.20 Å, 2V1K), **B**: Mb intermediate H (resolution 1.30 Å, 2V1E), **C**: peroxyMb (resolution 1.30 Å). All at pH 6.8.

Figure 4 - The haem regions shown with key residues of the crystal structure of **A**: sperm whale oxyMb (resolution 1.25 Å, 2Z6S), **B**: sperm whale peroxyMb (resolution 1.20 Å, 2Z6T), **C**: horse heart peroxyMb (resolution 1.30 Å, XXXX), **C**: oxyP450 (resolution 1.9 Å, 2VLX), **D**: hydroperoxyCPO / compound 0 (resolution 1.75 Å, 2J5M), **D**: compound III HRP (resolution 1.6 Å, 1H57).

Figure 5 – Crystal structure of Mb and P450 states during irradiation. In **A**, **B**, **C**: Crystal structures of the haem regions of Mb shown with the electron density $2F_o$-F_c map (contoured at 1σ in golden), the final F_o-F_c map (at +3σ in green and at -3σ in red) and difference F_o-F_c map with the peroxy/hydroxy atoms and extra water molecule omitted for map calculation (at 4σ in blue). Consecutive datasets collected on the same crystal: **A**: Dataset 1 – compound III (resolution 1.60 Å) (dose estimated to ~3 MGy), **B**: Dataset 2 – peroxyMb (resolution 1.50 Å) (dose estimated to ~10 MGy), **C**: annealing before collecting Dataset 3 – radiation-induced compound II (intermediate H) (resolution 1.60 Å) (dose estimated to ~12 MGy). In **D**, **E**: Crystal structure of haem regions of P450 shown with the electron density $2F_o$-F_c map (contoured at 1σ in golden) calculated by the Electron Density Server at Uppsala University [130], **D**: oxyP450 (1DZ8), **E**: oxyP450 after irradiation with 1.5 Å wavelength resulting in P450 compound I (1DZ9).

Figure 6 – Spin density (yellow) of the peroxy–HIE complex.

Figure 7 – The QM system of the quantum-refined structures for the seven possible states of the oxy, peroxy, and hydroperoxy complexes with a model of the distal His residue: **A:** oxy–HIE, **B:** oxy–HIP, **C:** peroxy–HIE, **D:** peroxy–HIP, **E:** hydroperoxy–HID, **F:** hydroperoxy–HIE, and **G:** hydroperoxy–HIP.

FIGURE 1

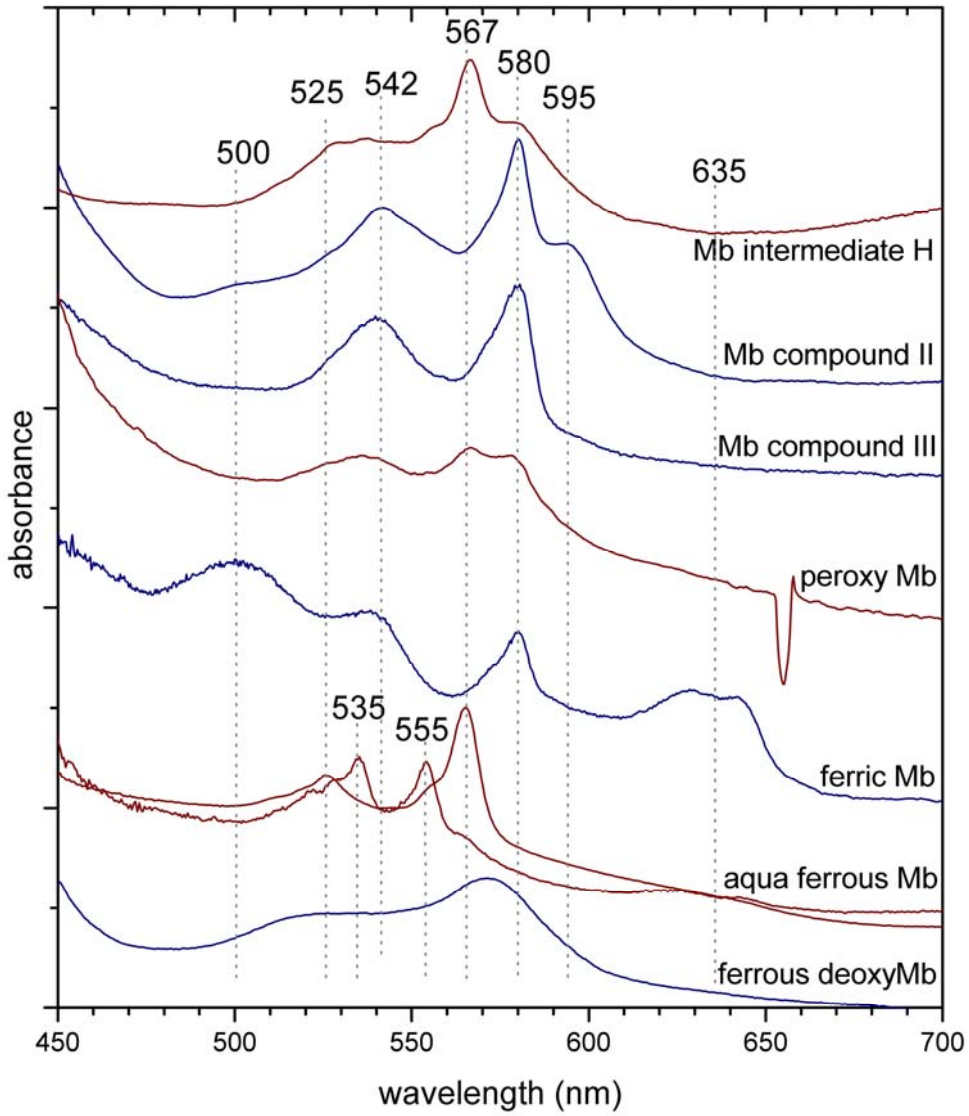
567
580
525
542
595
500
635
Mb intermediate H
Mb compound II
Mb compound III
peroxy Mb
535
555
ferric Mb
aqua ferrous Mb
ferrous deoxyMb
absorbance
450
500
550
600
650
700
wavelength (nm)

FIGURE 2AB

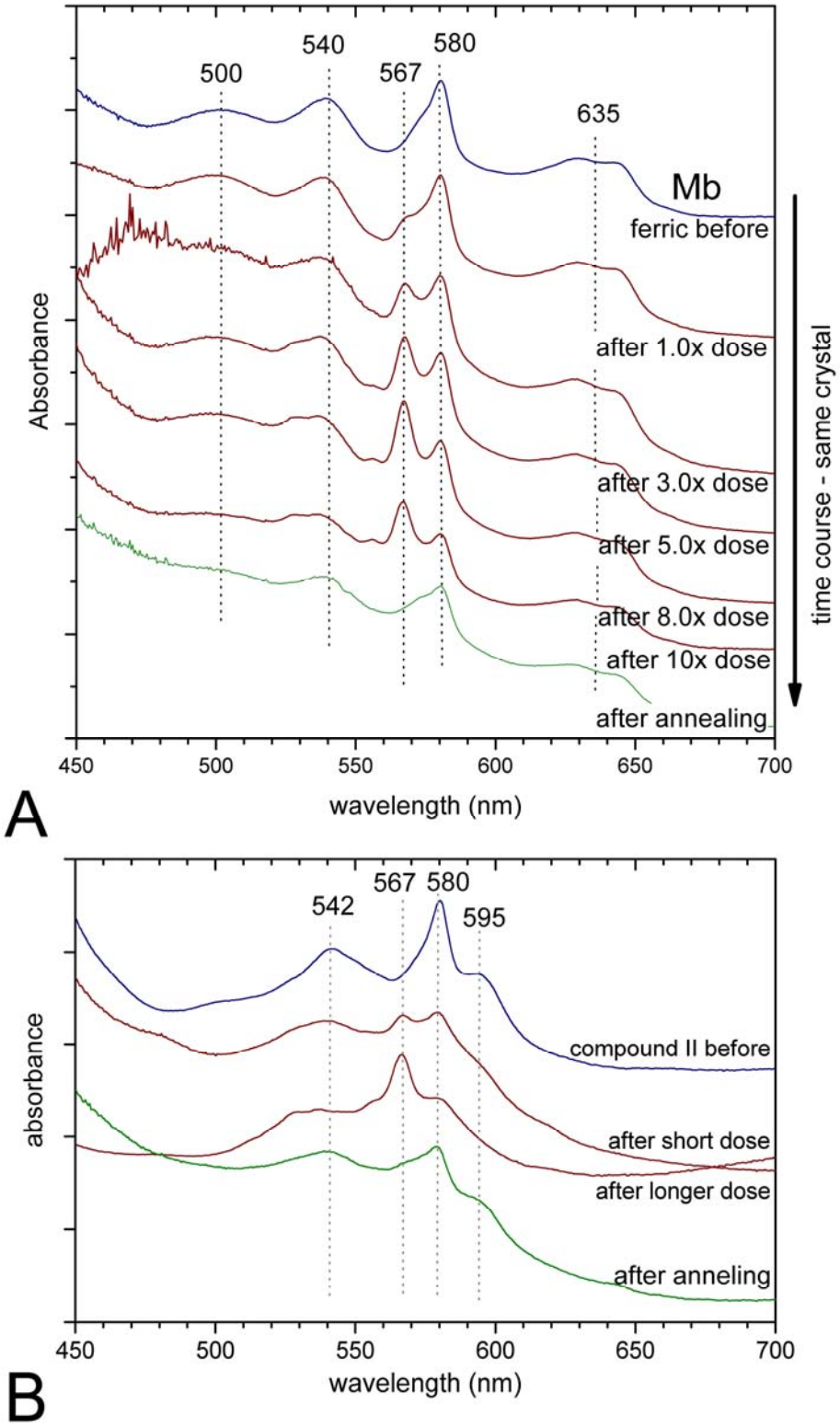
500
540
567
580
635
Mb
ferric before
after 1.0x dose
after 3.0x dose
after 5.0x dose
after 8.0x dose
after 10x dose
after annealing
time course - same crystal
Absorbance
450
500
550
600
650
700
wavelength (nm)
A
542
567
580
595
compound II before
after short dose
after longer dose
after anneling
absorbance
450
500
550
600
650
700
wavelength (nm)
B

FIGURE 2CD

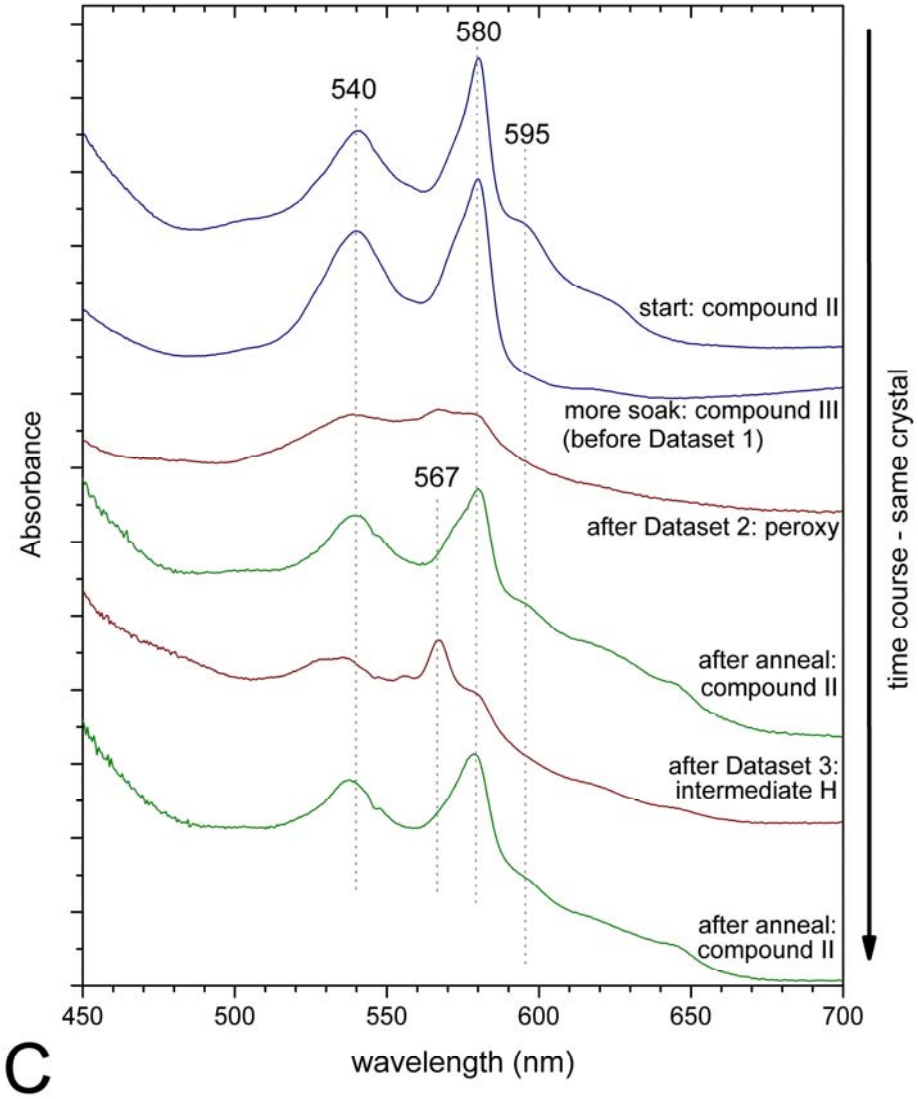
580
540
595
start: compound II
more soak: compound III
(before Dataset 1)
567
after Dataset 2: peroxy
after anneal:
compound II
after Dataset 3:
intermediate H
after anneal:
compound II
time course - same crystal
Absorbance
450
500
550
600
650
700
wavelength (nm)
C

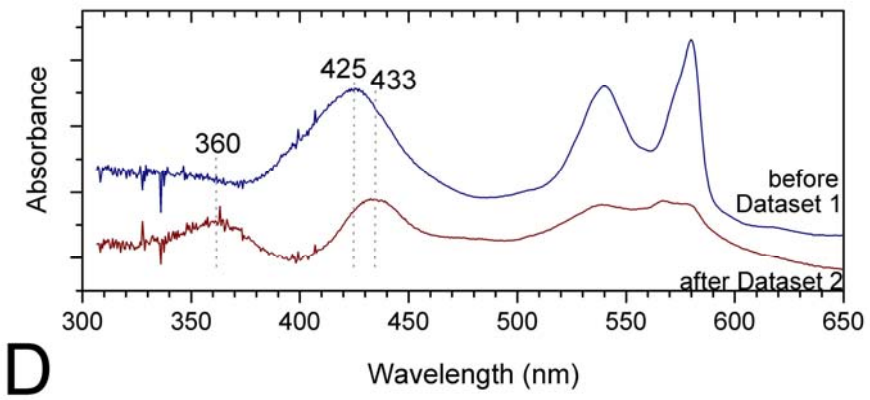
425
433
360
before
Dataset 1
after Dataset 2
Absorbance
300
350
400
450
500
550
600
650
Wavelength (nm)
D

FIGURE 3

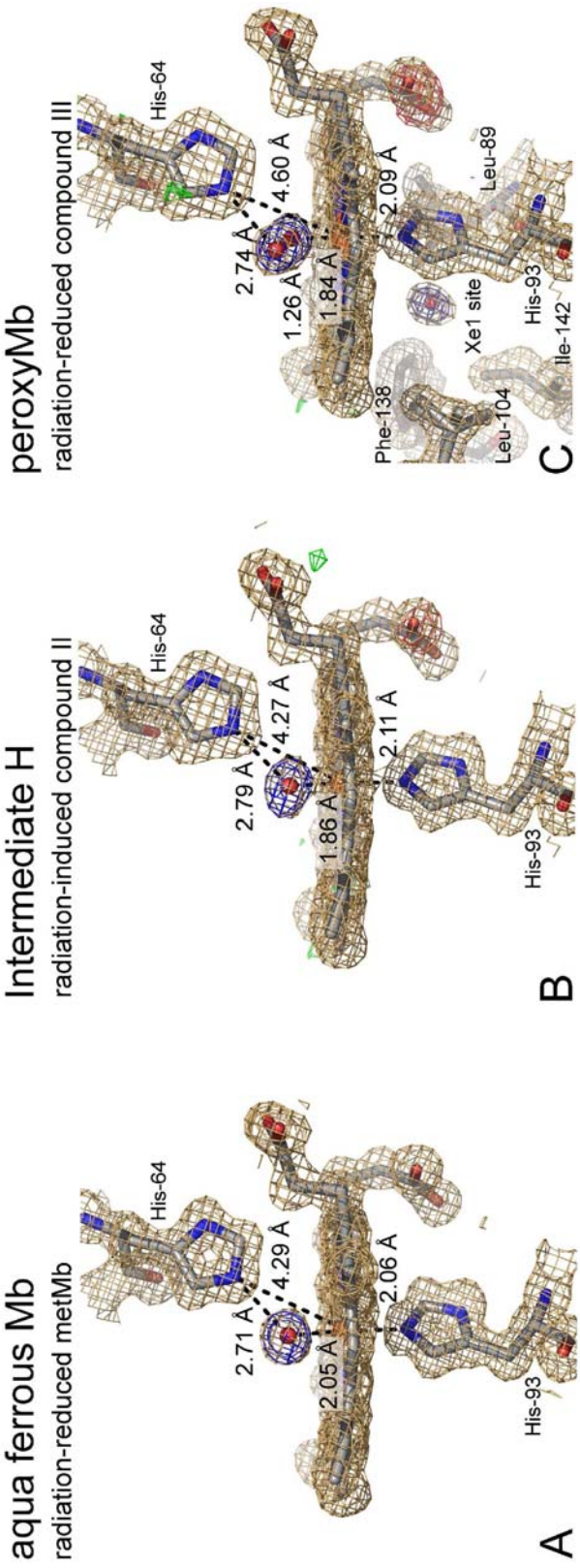
aqua ferrous Mb
radiation-reduced metMb
His-64
2.71 Å
4.29 Å
2.06 Å
2.05 Å
His-93
A
Intermediate H
radiation-induced compound II
His-64
2.79 Å
4.27 Å
2.11 Å
1.86 Å
His-93
B
peroxyMb
radiation-reduced compound III
His-64
2.74 Å
4.60 Å
2.09 Å
1.26 Å
1.84 Å
Leu-89
Xe1 site
His-93
Ile-142
Phe-138
Leu-104
C

FIGURE 4

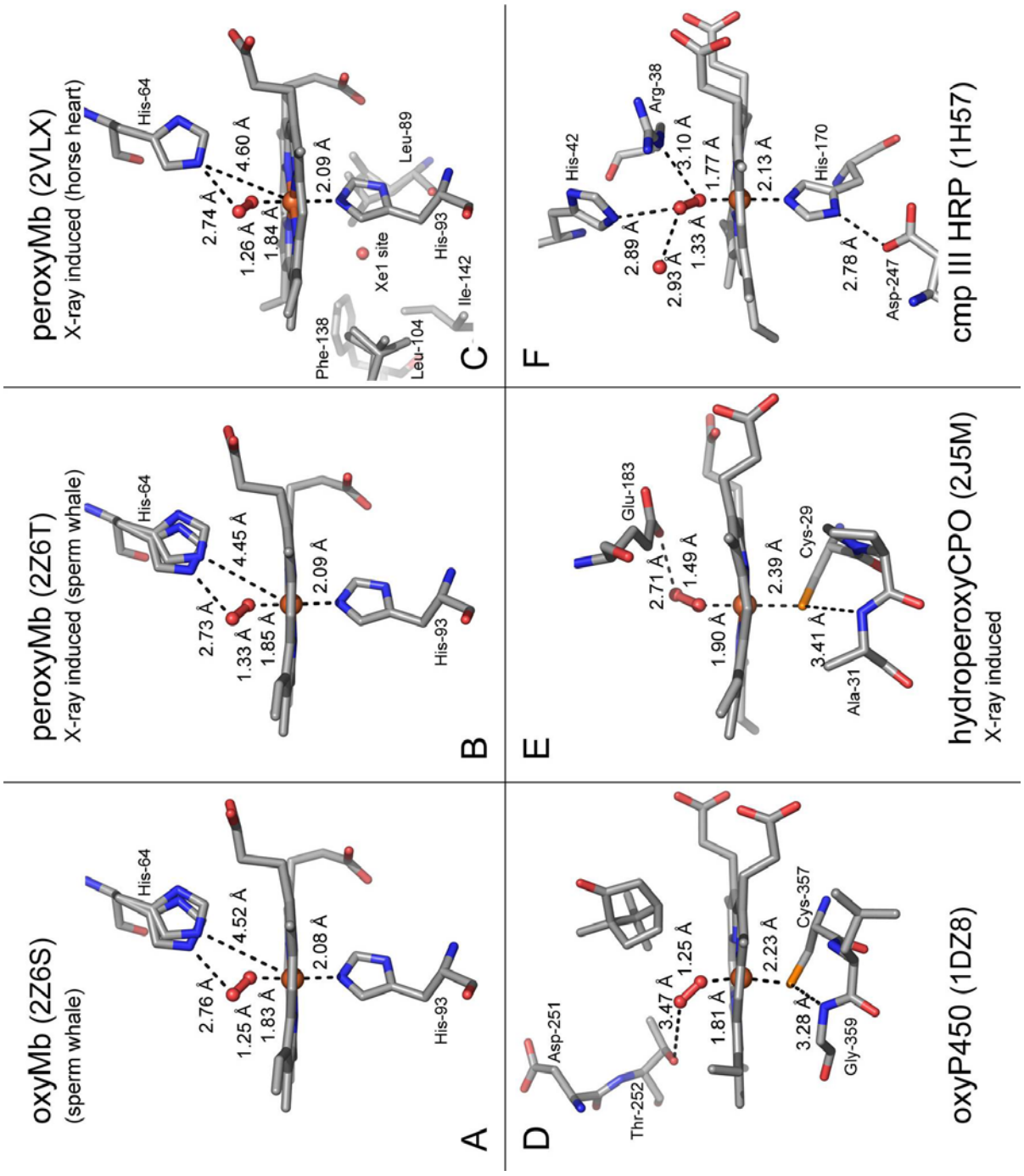
oxyMb (2Z6S)
(sperm whale)
peroxyMb (2Z6T)
X-ray induced (sperm whale)
peroxyMb (2VLX)
X-ray induced (horse heart)
hydroperoxyCPO (2J5M)
X-ray induced
cmp III HRP (1H57)
oxyP450 (1DZ8)
A
B
C
D
E
F
His-64
His-93
Xe1 site
Leu-89
Leu-104
Phe-138
Ile-142
Glu-183
Cys-29
Ala-31
Arg-38
His-42
His-170
Asp-247
Asp-251
Thr-252
Cys-357
Gly-359

FIGURE 5

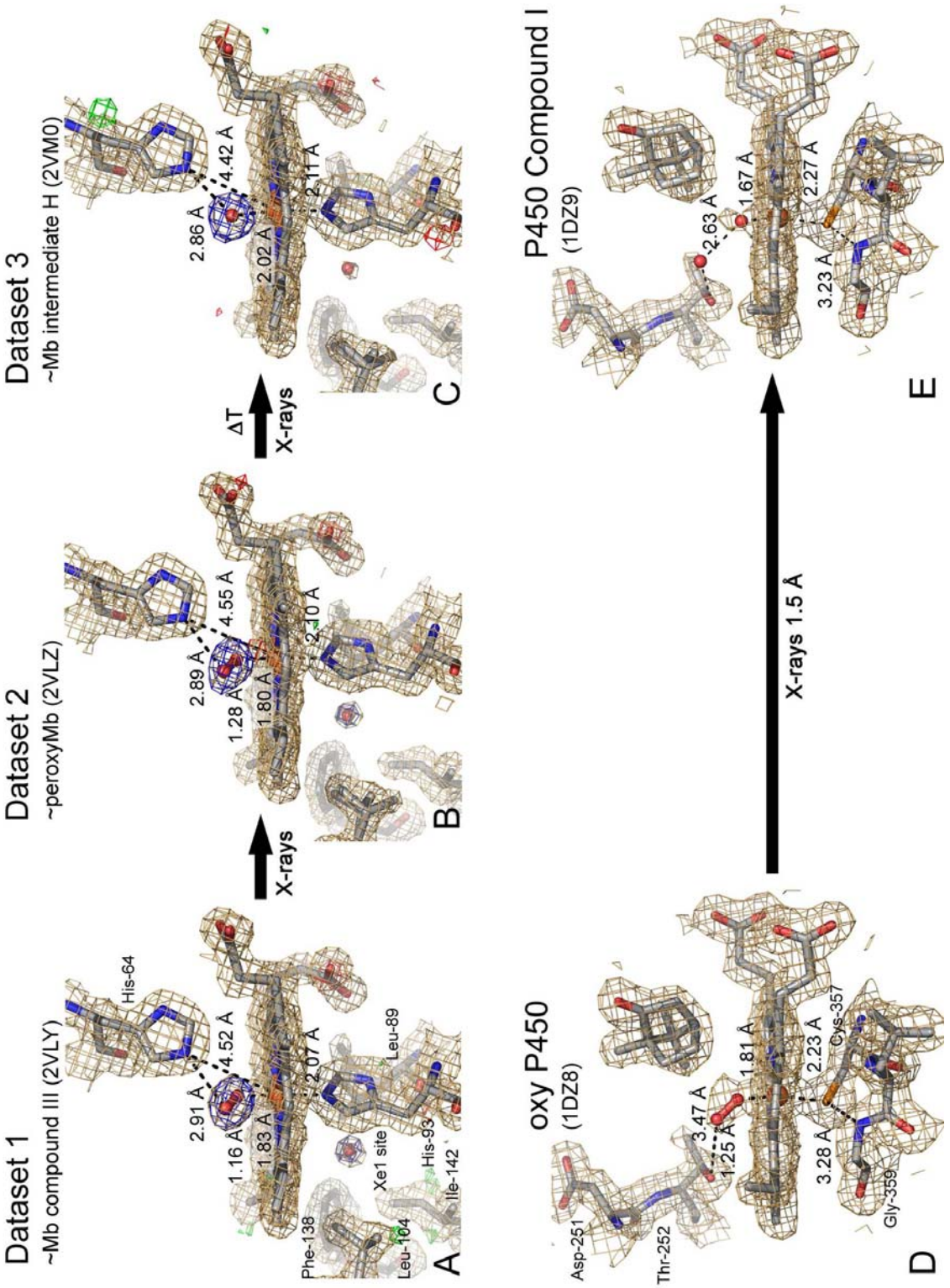
Dataset 1
~Mb compound III (2VLY)
Dataset 2
~peroxyMb (2VLZ)
Dataset 3
~Mb intermediate H (2VM0)
X-rays
X-rays
ΔT
P450 Compound I
(1DZ9)
oxy P450
(1DZ8)
X-rays 1.5 Å
His-64
Leu-89
Xe1 site
His-93
Ile-142
Phe-138
Leu-104
Asp-251
Thr-252
Cys-357
Gly-359
A
B
C
D
E

FIGURE 6

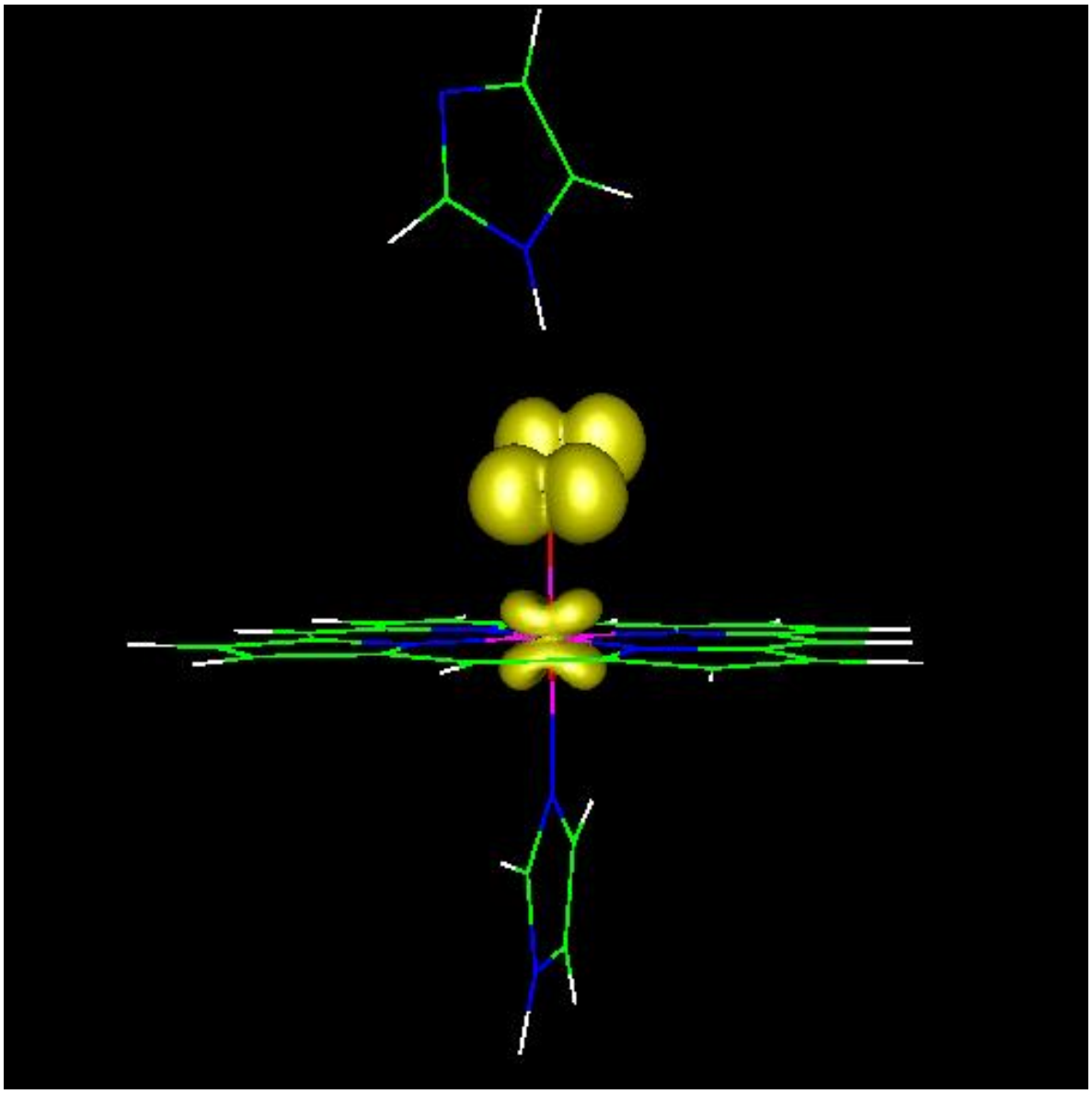

FIGURE 7